Published in final edited form as:
Microcirculation. 2014 November ; 21(8): 677–687. doi:10.1111/micc.12146.

Impact of Increased Intramuscular Perfusion Heterogeneity on Skeletal Muscle Microvascular Hematocrit in the Metabolic Syndrome

Joshua T. Butcher[1,2], **Shyla C. Stanley**[1,2], **Steven D. Brooks**[1,2], **Paul D. Chantler**[1,3], **Fan Wu**[4], and **Jefferson C. Frisbee**[1,2]

[1]Center for Cardiovascular and Respiratory Sciences, West Virginia University Health Sciences Center, Morgantown, WV

[2]Department of Physiology and Pharmacology, West Virginia University Health Sciences Center, Morgantown, WV

[3]Division of Exercise Physiology, West Virginia University Health Sciences Center, Morgantown, WV

[4]Novartis Institutes for BioMedical Research, Drug Metabolism and Pharmacokinetics, East Hanover, NJ

Abstract

Objective—To determine microvascular hematocrit (H_{MV}) and permeability-surface area product (PS) in skeletal muscle of obese Zucker rats (OZR) and evaluate the impact of increased microvascular perfusion heterogeneity on mass transport/exchange.

Methods—The *in situ* gastrocnemius muscle from OZR and lean Zucker rats (LZR) was examined under control conditions and following pre-treatment with TEMPOL (antioxidant)/ SQ-29548 (PGH_2/TxA_2 receptor antagonist), phentolamine (adrenergic antagonist), or all agents combined. A spike input of a labelled blood tracer cocktail was injected into the perfusing artery. Tracer washout was analyzed using models for H_{MV} and PS. Individual capillary hematocrit (H_T) was determined in *in situ* cremaster muscle of OZR and LZR using videomicroscopy.

Results—H_{MV} was decreased in OZR vs. LZR. While TEMPOL/SQ-29548 or phentolamine had minor effects, treatment with all three agents improved H_{MV} in OZR. H_T was not different between strains, although variability was increased in OZR, and normalized following treatment with all three agents. PS was reduced in OZR and was not impacted by intervention.

Conclusions—Increased microvascular perfusion heterogeneity in OZR reduces H_{MV} in muscle vascular networks and increases its variability, potentially contributing to premature muscle fatigue. While targeted interventions can ameliorate this, the reduced microvascular surface area is not acutely reversible.

Send Correspondence to: Jefferson C. Frisbee, Ph.D., Center for Cardiovascular and Respiratory Sciences, Department of Physiology and Pharmacology, Robert C. Byrd Health Sciences Center, PO Box 9105, West Virginia University School of Medicine, Morgantown, WV 26505, Phone: (304) 293-6527, Fax: (304) 293-5513, jefrisbee@hsc.wvu.edu.

Keywords

microcirculation; peripheral vascular disease; rodent models of metabolic syndrome; regulation of skeletal muscle blood flow; microvascular hemodynamics

Introduction

One of the major negative health outcomes associated with chronic presentation of the metabolic syndrome is a significantly increased risk for the development of peripheral vascular disease (3, 18, 30) and perfusion insufficiency within the microcirculation (6, 12). What makes this especially compelling is that the metabolic syndrome, defined as the combined presentation of multiple systemic pathologies including obesity, impaired glycemic control, hypertension and atherogenic dyslipidemia, is a condition wherein the risk for negative outcomes is greater than a simple summation of the risks associated with the individual constituent pathologies (10, 26). The obese Zucker rat (OZR), a model for the metabolic syndrome, has the origin of this condition in a genetic mutation for severe leptin resistance, resulting in chronic hyperphagia and the ensuing development of the systemic pathologies listed above (1, 11). However, OZRs develop the functional characteristics of peripheral vascular disease (e.g., premature muscle fatigue, poor exercise performance [12]) in the absence of significant development of atherosclerotic plaques or lesions; thus implicating impairments to microvascular regulation of blood flow as a critical contributor to poor muscle performance outcomes.

Our ongoing studies have demonstrated that classic markers of peripheral vascular dysfunction, such as impaired vascular reactivity and compromised endothelial function, are not strong, consistent predictors of either poor perfusion or muscle performance outcomes in OZR (12). Continuing investigation has revealed that an increased heterogeneity in the spatial distribution of blood flow at arteriolar bifurcations, iterated from proximal resistance arterioles to pre-capillary terminal microvessels is a far stronger and more consistent predictor of impaired functional outcomes (13). Further, our most recent evidence suggests that this increased spatial heterogeneity of intramuscular perfusion distribution is actually exacerbated (as opposed to being compensated for) by a reduced level of temporal switching at bifurcations in skeletal muscle microvascular networks in OZR (5). Taken together, these processes create a condition wherein perfusion distribution within skeletal muscle microvascular networks becomes increasingly heterogeneous with progression of the metabolic syndrome and that the flexibility of the system to alter perfusion distribution in response to imposed challenges (such as elevated metabolic demand) is blunted. While we have simulated the impact of these iterative alterations in blood flow distribution at bifurcations on pre-capillary perfusion distribution within skeletal muscle (13), there are no experimentally-determined outcomes of these processes on critical components of mass transport and exchange within skeletal muscle of OZR. Acute intervention with phentolamine (adrenoreceptor antagonist) was effective at restoring perfusion distribution characteristics in the proximal levels of the skeletal muscle microvascular networks only. However, correcting vascular endothelial dysfunction with a combination therapy of an anti-oxidant (TEMPOL) and a blocker of the PGH_2/TxA_2 receptor (SQ-29548) was primarily

effective at restoring normal perfusion distribution patterns in the distal levels of the microvascular networks (5, 13). These previous results strongly suggest that the ultimate determinants of microvascular perfusion and muscle performance outcomes contribute in a synergistic fashion that must be taken into consideration.

One of the key parameters associated with mass transport and exchange in the distal microcirculation is microvascular hematocrit (15, 20, 31), as the population and distribution of erythrocytes within the distal microcirculation and capillary networks represents a critical contributor to not only tissue oxygenation, but also for the removal of metabolic end-products. While, based on the cumulative impact of the network and vessel Fahraeus effects (19, 27), we can predict that alterations to microvascular hematocrit (H_{MV}) will track with alterations to the spatial distributions of perfusion (28), this has not been demonstrated. In the present study, we employ two methods for determining microvascular hematocrit at both the individual and whole network levels of resolution in LZR and OZR under control conditions and in response to a series of interventions that have been demonstrated to not only improve perfusion outcomes, but also muscle fatigue resistance. In addition, we determine the permeability-surface area product (PS) across the skeletal muscle microcirculation using the established Crone/Renkin Model (7, 16), as an indicator of the total area available for capillary exchange under the conditions of the present study. This study tested the hypothesis that H_{MV}, while not reduced, is increasingly heterogeneous in the skeletal muscle of OZR relative to LZR, and that this may represent a critical contributor to the poor muscle performance outcomes that have been previously determined in OZR at this age (12). A secondary hypothesis was that PS is significantly reduced within skeletal muscle of OZR relative to LZR and, as this represents structural alterations to microvessel density in OZR with development of the metabolic syndrome (14), this is not improved by any acute intervention.

Materials and Methods

Animals—Male lean (total n=12) and obese Zucker rats (total n=39), purchased from Harlan, were fed standard chow and drinking water *ad libitum* and were housed in the animal care facility at the West Virginia University Health Sciences Center. All protocols received prior IACUC approval. At ∼17 weeks of age, rats were anesthetized with injections of sodium pentobarbital (50 mg/kg, i.p.), and received tracheal intubation to facilitate maintenance of a patent airway. In all rats, a carotid artery and an external jugular vein were cannulated for determination of arterial pressure and for infusion of supplemental anesthetic and pharmacological agents, as necessary. Any animal in which mean arterial pressure was found to be below 85 mmHg, or where MAP had decreased by more than 15% from that following equilibration (without any pharmacological intervention) was not used in the present study. Blood samples were drawn from the venous cannula for determination of glucose and insulin concentrations (Millipore, Billerica, MA) as well as cholesterol/triglyceride levels (Wako Diagnostics, Richmond, VA), and nitrotyrosine (Oxis International. Foster City, CA). Blood gases were determined using a Corning RapidLab 248 Blood Gas Analyzer (Siemens Medical Solutions, Malvern, PA). Unless otherwise noted, all drugs and chemicals were purchased from Sigma-Aldrich (St. Louis, MO).

Preparation of In Situ Cremaster Muscle—In one cohort of rats (LZR n=6; OZR n=14), an *in situ* cremaster muscle was prepared for study using intravital microscopy as described previously (21). After completion of the *in situ* cremaster muscle preparation, the tissue was continuously superfused with physiological salt solution (PSS) equilibrated with a 5% CO_2-95% N_2 gas mixture, and maintained at 35°C as it flowed over the muscle. The ionic composition of the PSS was as follows (mM): NaCl 119.0, KCl 4.7, $CaCl_2$ 1.6, NaH_2PO_4 1.18, $MgSO_4$ 1.17, $NaHCO_3$ 24.0, and disodium EDTA 0.03. Succinylcholine chloride (0.1 mM) was added to the superfusion solution to prevent spontaneous contractions of the cremaster muscle.

Capillary tube hematocrit (H_T) was determined by counting the number of erythrocytes within a measured capillary segment from still images, with final H_T measures representing the mean of multiple determinations made during data collection periods. The calculation of H_T used the following equation (8, 9):

$$H_T = (n \bullet MCV \bullet 100)/[\pi \bullet (D/2)^2 \bullet L]$$

where n represents the number of erythrocytes in a given length of capillary (L), MCV and D represents mean corpuscular volume (72 μm^3) and capillary diameter (6.7 μm), respectively (17). Data were collected under control conditions in LZR and OZR, and following treatment of the *in situ* cremaster muscle with the anti-oxidant TEMPOL (10^{-3} M) combined with the TxA_2 receptor antagonist SQ-29548 (10^{-4} M), and/or the α_1/α_2 adrenergic receptor antagonist phentolamine (10^{-5} M); within the superfusate solution. No cremaster muscle was exposed to all interventions in order to avoid compromising data quality owing to experiments of excessive duration. In addition to the collection of responses under control conditions, individual cremaster preparations were exposed to a maximum of three interventions, each separated by ~30 minutes of washout. Treatment or washout effectiveness was verified by determining abolition or recovery of mechanical responses following challenge with appropriate agonists (e.g., the α_1 adrenergic agonist phenylephrine, the stable TxA_2 mimetic U-46619, and the endothelium dependent dilator agonist acetylcholine). Maximum experimental duration from preparation to termination was approximately four hours, after which time all animals were humanely euthanized by an intravenous overdose of anesthetic followed by a bilateral pneumothoracotomy.

Preparation of In Situ Blood Perfused Hindlimb—In a separate set of LZR (n=6) and OZR (n=24), the left hindlimb of each animal was isolated *in situ* (13) with minor modifications. Heparin (500 IU/kg) was infused via the jugular vein to prevent blood coagulation. Subsequently, an angiocatheter was inserted into the femoral artery, proximal to the origin of the gastrocnemius muscle to allow for bolus tracer injection. Additionally, a small shunt was placed in the femoral vein draining the gastrocnemius muscle that allowed for diversion of flow into a port which facilitated sampling of the venous effluent. Finally, a microcirculation flow probe (Transonic; 0.5/0.7 PS) was placed on the femoral artery to monitor muscle perfusion. Upon completion of the surgical preparation, the gastrocnemius muscle was allowed 30 minutes of self-perfused rest. In individual experiments, rats

received intravenous infusion of phentolamine (10 mg/kg) and/or the combination of TEMPOL (50 mg/kg) and SQ-29548 (10 mg/kg). Effectiveness of these interventions was assessed by monitoring the changes in arterial pressure in response to intravenous infusion of phenylephrine (10 μg/kg), methacholine (10 μg/kg) or U-46619 (10 μg/kg), respectively.

In Vitro Erythrocyte/Plasma Labeling

Tracers for three biological volumes: the intravascular axial cylinder (^{51}Cr erythrocytes), the complete plasma volume (^{125}I-albumin), and the extravascular volume (^{86}Rb) were produced for these experiments. The procedure for labeling erythrocytes followed that described previously, with minor modification (4, 22). Briefly, from homologous donor rats, 2 ml of heparin-treated blood was removed and incubated for one hour with 20 μCi of sodium ^{51}chromate. Subsequently, the blood was centrifuged for 5 minutes at 1375 g and the supernatant removed. This procedure has been shown to be effective in removing more than 90% of the unbound chromium (4). The labeled erythrocytes were then re-suspended in PSS to the animal's systemic arterial hematocrit (H_{SYS}) as determined from a spun arterial blood sample taken during the initial surgical preparation. 2 μCi of ^{125}iodine labeled albumin was then added to the red cell suspension and allowed to equilibrate in a gently stirred beaker for 30 minutes. Finally, 10 μCi of ^{86}rubidium chloride was added to the erythrocyte solution prior to usage. All radionuclides were purchased from Perkin-Elmer (Shelton, CT). For the estimate of H_{MV}, ^{125}I-albumin was used as the diffusing tracer while the ^{51}Cr-erythrocytes were used as the reference. For the estimate of PS, the labeled albumin served as the reference, while the ^{86}Rb was used as the diffusing tracer.

Tracer Injection and Collection Procedures—For each injection of the tracer combination, 20 μl of red blood cell suspension with the three labels was injected as a spike bolus (injection time <0.5 s) into the arterial angiocatheter and venous effluent samples were collected at a rate of 1/s for the subsequent 35 seconds. Venous effluent samples were immediately transferred into silicate tubes and placed into a gamma counter for activity determination (activity levels were subsequently corrected for overlap and normalized to the injectate reference). Each rat received an intravenous infusion of unlabeled homologous donor erythrocytes suspended in PSS at the individual animal's hematocrit (∼45%) to replace the lost volume, and this was allowed a minimum of 20 minutes for circulation prior to subsequent intervention. In order to assess the potential for leakage of the labeled albumin from the intravascular space as a source for error, the gastrocnemius muscle was cleared by perfusion with physiological salt solution following euthanasia. Subsequent to a determination of mass, the muscle was placed in the counter for determination of residual activity. Residual activity within the gastrocnemius muscle did not exceed 200 cpm/animal; a level that was far lower than those determined in the venous blood aliquots. All protocols had received prior approval from the Radiation Safety Office at the WVU Health Science Center.

Data and Statistical Analyses

Computing permeability-surface product (PS)—Permeability-surface product (PS) values are estimated from washout curves of plasma albumin bound ^{125}I (as the reference tracer) and the extravascular ^{86}Rb (as the diffusible tracer), based on the Crone/Renkin

model (2). The Crone/Renkin model was implemented in Excel. Briefly, the time courses of tracer concentrations were normalized to the reference concentrations and then the peak time (t_{peak}) was found at the maximum concentration of the reference tracer. From the normalized tracer time courses, the net extraction ratio was computed as:

$$E_{net}(t)=1-\int_0^t h_D(s)ds/\int_0^t h_R(s)ds,$$

where h_D and h_R denotes the transport functions for the diffusible and reference tracers, respectively (2). The extraction ratio (E) was assumed to be equal to $E_{net}(t)$ at t_{peak}, i.e.,

$$E=E_{net}(t_{peak}).$$

Since the reference tracer (I-125) is bound to plasma albumin, the flow of solutes was computed as:

$$F_s=Flow\cdot Mass\cdot(1-H_{SYS}),$$

where *Flow* denotes the measured blood flow per tissue mass, *Mass* denotes the weight of muscle used in experiments, and H_{SYS} denotes the systemic hematocrit. Finally, the classical Crone-Renkin equation was applied to compute the permeability-surface product of capillaries (PS_c):

$$PS_c=-F_s\cdot \mathrm{In}(1-E).$$

Estimating microvascular hematocrit—Microvascular hematocrit (H_{MV}) was estimated from washout curves of ^{51}Cr-labeled red blood cell and ^{125}I-labeled plasma albumin based on the Overholser model (22), which was implemented in Excel (Microsoft, Redmond, WA). In this case, ^{51}Cr serves as the reference tracer, while ^{125}I serves as the diffusible tracer. With concentrations of the reference and diffusible tracers indicated as C_R and C_1, respectively, the Overholser model states that the following relationship exists:

$$C_1(t-\tau)=h_r^{'}\cdot C_R\left((t-\tau)h_r^{'}\right),$$

where $h_r^{'}$ denotes the modified ratio of H_{MV} to large-vessel or systemic hematocrit (H_{SYS}), τ denotes the appearance time at which the reference tracer concentration first exceeds 1% of its peak value. The parameter $h_r^{'}$ was estimated by fitting experimentally measured washout curves of the reference and diffusible tracers to the above relationship. Then h_r, the actual ratio of H_{MV} to H_{SYS}, was computed as:

$$h_r = \frac{h_r'}{1 + H_{SYS} \cdot h_r' - H_{SYS}}.$$

The value of H_{MV} was obtained based on the definition of h_r, i.e.,

$$H_{MV} = h_r \cdot H_{SYS}.$$

Estimating Oxygen Fluxes—The perfusive oxygen fluxes (Q_{O2}) in the skeletal muscle of LZR and OZR under the conditions of the current study are:

$$Q_{O2} = Flow \cdot CaO2,$$

where Flow refers to bulk flow per tissue mass, and CaO2 refers to oxygen content in arterial blood.

The diffusive oxygen transport flux in the skeletal muscle of LZR and OZR under the conditions of the current study is computed based on mass balance:

$$J_{O2} = Flow \cdot (CaO2 - CvO2),$$

where CvO2 refers to oxygen content in venous blood.

All data throughout the manuscript are presented as mean±SE. Statistically significant differences in measured and calculated parameters were determined using a one sample *t*-test (differences from zero), Student's *t*-test, Levene's test for homogeneity of variance, or analysis of variance (ANOVA) with Student-Newman-Keuls post-hoc test used as needed. In all cases, $p<0.05$ was taken to reflect statistical significance.

Results

Data describing the basic characteristics of the LZR and OZR used in the present study are summarized in Table 1. In addition to significant obesity and elevations in arterial pressure, plasma insulin, and nitrotyrosine levels were significantly greater in OZR than LZR.

Table 2 presents data describing the gastrocnemius muscle blood flow and blood oxygen levels in LZR and OZR under the conditions of the present study. These data are used for the determination of perfusive (Q_{O2}) and diffusive (J_{O2}) oxygen flux, using the equations described above.

Figure 1 presents representative washout curves, normalized to the injectate reference, from the three tracers across the gastrocnemius muscle of LZR (Panel A), OZR (Panel B), OZR + phentolamine (Panel C), OZR + TEMPOL/SQ-29548 (Panel D) and OZR + all three agents

(Panel E). As is evident by these tracer washout patterns, the initial appearance of all three tracers is faster in OZR, but there also remains a later retention of all three as well. Also evident is that the temporal differences in the tracer washout between the plasma (^{125}I-albumin) and extravascular (^{86}Rb) tracers determined in LZR were reduced in OZR. While treatment of OZR with either phentolamine (Panel C) or TEMPOL/SQ-29548 (Panel D) results in modest corrections to portions of the washout curves, combined treatment will all three agents (Panel E) produced the greatest restorative impact.

Data describing H_{MV} in LZR and OZR skeletal muscle under the conditions of the current study are summarized in Figure 2. Panel A presents the 'hematocrit reduction ratio (h_r)', as calculated from the kinetics of the washout curves for ^{51}Cr-erythrocytes (as the reference tracer) and ^{125}I-albumin (as the diffusing tracer) using the model described above and previously (22). The h_r was significantly reduced in OZR as compared to LZR, but was not significantly altered as a result of either treatment with phentolamine or TEMPOL/SQ-29548. However, pre-treatment of OZR with all three agents restored h_r, to the point where it was not different from that determined in LZR under control conditions. Similarly, as compared to LZR, aggregate H_{MV} within the gastrocnemius muscle of OZR was significantly reduced under control conditions. Following acute intervention with either phentolamine or TEMPOL/SQ-29548, H_{MV} was not significantly altered, while combined treatment of OZR with all three agents restored H_{MV} to levels comparable to that in LZR under control conditions (Panel B). In additional experiments, treatment of LZR with these agents did not result in a consistent, significant effect.

Figure 3 presents data describing H_T in individual microvessels within the present study. Using the *in situ* cremaster muscle preparation, to gain insight into the changes in H_T at a higher level of spatial resolution between LZR and OZR, it was evident that the average microvessel tube hematocrit (the hematocrit within a microvessel at a specific time) was not significantly reduced in OZR as compared to LZR (Panel A). However, the variability of H_T in OZR was significantly greater than that determined in LZR, indicating that the heterogeneity in H_T was elevated with the progression of the metabolic syndrome. While treatment with either phentolamine or TEMPOL/SQ-29548 resulted in modest improvements to the variability of H_T in OZR, combined treatment with all three agents restored H_T to the point where neither the mean nor the variance was different from that determined in LZR. These differences in the variance of H_T between LZR and OZR under the conditions of the present study can be clearly demonstrated when the data are presented as a box and whisker plot, where the distribution of values of H_T are clearly much wider in OZR (Panel B).

The changes in calculated peak extraction and PS product across the gastrocnemius muscle of LZR and OZR under the conditions of the present study are summarized in Figure 4. As shown in Panel A, the extraction at the peak washout time was not consistently or significantly altered between OZR and LZR under any conditions (Panel A). However, as a result of the changes in blood flow, calculated PS product in OZR remained significantly reduced below that for LZR, regardless of the imposed intervention and was not improved as compared to untreated conditions (Panel B).

Figure 5 summarizes the changes in perfusive oxygen flux (Q_{O2}; Panel A), diffusive oxygen flux (J_{O2}; Panel B) and the correlation between diffusive oxygen flux and PS product (Panel C) under the conditions of the present study. Q_{O2} was significantly reduced in OZR vs. LZR under control conditions, although treatment with phentolamine partially restored Q_{O2} levels toward that determined in LZR. Treatment with TEMPOL/SQ-29548 was without significant effect, either alone or in combination with phentolamine (Panel A). In contrast, J_{O2}, while also significantly reduced in OZR vs. LZR was improved with both phentolamine and TEMPOL/SQ-29548, although the total improvement was not back to the level determined in LZR under control conditions (Panel B). As shown in Panel C, the calculated diffusive oxygen flux (J_{O2}) is correlated with computed PS product in an approximately linear relationship for both LZR and OZR, under control conditions and following the interventions.

Discussion

This study builds on a series of recent efforts that begin to define the actual microvascular contribution to the functional manifestation of non-atherosclerotic peripheral vascular disease in the OZR model of the metabolic syndrome; specifically attempting to link integrated regulation of blood flow with microvascular hemodynamics to determine potential limitations to the ability of skeletal muscle to resist fatigue. Our earlier work (12) revealed that vascular dysfunction, and the associated impairments to perfusion within skeletal muscle of OZR with elevated metabolic demand, was a reflection to two processes: (1) a dysregulation of adrenergic control over perfusion resistance and metabolic sympatholysis that constrains bulk blood flow through the proximal microcirculation and (2) the increasing importance of endothelial dysfunction within the distal microcirculation, primarily through oxidant stress and the production of thromboxane A_2, which compromises perfusion:demand matching, impairing aggregate oxygen extraction and uptake (VO_2).

Building on this concept, we demonstrated that these two processes create a condition within the skeletal muscle microcirculation of OZR that is defined by an increasing heterogeneity of erythrocyte distribution (γ) at arteriolar bifurcations (13). The underlying contribution to increased γ was dominated in the proximal microcirculation by altered adrenergic behavior in OZR versus LZR, and could be ameliorated through adrenoreceptor blockade with phentolamine. However, in the distal microcirculation, this adrenergic contribution was muted, while the impact of endothelial dysfunction was more functionally relevant; although it was correctable by treatment with antioxidants or thromboxane receptor blockade. A simulation of the impact of alterations to γ at successive arteriolar bifurcations indicated that perfusion heterogeneity at the pre-capillary level would be dramatically increased owing to cumulative upstream effects (13). Finally, our recent work suggests that the increased γ at arteriolar bifurcations is not only a process for which there is no apparent compensation, which would most likely be in the form of increased ‘temporal switching’ of the high-γ and low-γ pathways between parallel daughter arterioles, but that it is exacerbated under the conditions in OZR such that a heterogeneous perfusion distribution is maintained and is relatively insensitive to modulation (5).

While compelling, these previous results only take on meaningful biological significance if the processes of mass transport/exchange within the skeletal muscle microcirculation of OZR are compromised as a result. Two of the most critical contributors to the overall regulation of microvascular mass transport/exchange are hematocrit within the microvasculature (H_{MV} or H_T) and the surface area available for gas/substrate exchange, estimated using permeability-surface area product (PS). Using established tracer washout models for determining both H_{MV} (22) and PS (2), we utilized the washout kinetics for an erythrocyte tracer (^{51}Cr-RBC), an intravascular tracer (^{125}I-albumin) and an extravascular tracer (^{86}Rb) to determine both parameters for the *in situ* gastrocnemius muscle of OZR and LZR. Further, to provide data at a highest relevant level of resolution for microvascular hematocrit (the individual microvessel), we employed intravital microscopy of the *in situ* cremaster muscle of OZR and LZR to directly count erythrocytes and calculate H_T within individual microvessels.

Using the tracer washout methodology, the major observation was that aggregate H_{MV} within skeletal muscle of OZR was reduced below that in LZR. While intervention with either the adrenoreceptor antagonist (phentolamine) or agents targeted improving endothelial function (TEMPOL/SQ-29548) did not improve H_{MV} in skeletal muscle of OZR, combined treatment with all three agents resulted in a significant improvement, to a level that was not significantly different from that in LZR. However, supports our more global observation, as this combination intervention has also consistently been able to cause the greatest improvement to muscle fatigue resistance (12) and microvascular perfusion distribution (γ) in skeletal muscle of OZR (13).

The determination of H_T at a higher level of resolution (the individual microvessel) revealed additional insights that were not accessible using a tracer washout protocol. While results were directionally consistent to those for H_{MV}, the divergence in mean values of H_T within individual microvessels was blunted between OZR and LZR, under both control and treated conditions. However, what was striking, and is presented most clearly in Figure 3, Panel B, is that the variability in H_T between individual microvessels within a network in OZR skeletal muscle is increased over that in LZR. As above, treatment with either the adrenoreceptor antagonist or agents against endothelial dysfunction had a modest impact on the variability of H_T, although treatment with all three agents was most successful at restoring the variability in H_T within the network.

Taken together, these results are important in terms of placing our previous observations in the proper context. Under control (untreated) conditions in OZR, the accumulated effect of the increased γ at successive bifurcations is increased perfusion heterogeneity at the pre-capillary level (13). This accumulated effect, largely a reflection of the network Fahraeus effect (27, 28) and the tendency for erythrocytes to disproportionately follow the pathway of highest blood flow, will have the cumulative impact of not only reducing H_{MV} at any level of the microcirculation in OZR versus LZR, it will also produce an increase in the variability of H_T between microvessels within a network for OZR. The combination of this increased spatial heterogeneity in terms of erythrocyte distribution within microvascular networks of OZR, combined with an attenuated ability of networks to compensate for the increased heterogeneity (5), has the potential to severely compromise mass transport and exchange

within the distal microcirculation. If present under conditions of elevated metabolic demand, this combination of effects may represent a significant contributing factor to the poor performance determined in contracting skeletal muscle of OZR.

One of the key observations from the present study was that PS product, reduced in OZR versus LZR was not significantly altered by any imposed intervention. This is a particularly interesting result in that it clearly suggests that there are ‘ceilings’ for capillary surface area that are not alterable in an acute time frame, and that these may act as a significant constraint on muscle perfusion distribution (or, if present, to muscle performance with elevation in metabolic demand). Previous results also suggested that this was the case based on whole muscle hemodynamics, where perfusion resistance across the muscle at multiple metabolic demands was elevated in OZR versus LZR and, this elevation in resistance was maintained even under conditions of pharmacological treatment causing maximum vasodilation (12, 14). It is likely that this reduction in capillary surface area primarily reflects the progressive rarefaction of the skeletal muscle microvessel networks and the reduction in capillary density in OZR manifesting the metabolic syndrome (14). As a structural alteration, this would not represent a contributor to the poor perfusion and muscle performance outcomes in OZR that would be susceptible to therapeutic interventions in the acute time frame.

Previous results addressing microvascular transport, erythrocyte flux and oxygenation in conditions of cardiovascular disease or disease risk are relevant for interpretating the results of the present study. In type 2 diabetes mellitus, similar to the results of the present study, both the convective and diffusive oxygen transport within the microcirculation of *in situ* spinotrapezius muscle of the Goto-Kakizaki rat were reduced below that in control animals (23). In a follow up study, those authors demonstrated that the reduced oxygen fluxes in the GK rat could impair oxygen exchange in the microcirculation and potentially impair skeletal muscle performance (24). Comparable results have also been identified in models of chronic heart failure as well (25, 29). While results from the present study were collected under resting conditions, given these previous results, it is certainly likely that impairments to perfusive and diffusive oxygen fluxes in the skeletal muscle microcirculation of OZR versus LZR could have the potential to impair tissue oxygenation and muscle performance under conditions of elevated metabolic demand.

When integrated with those from our recent efforts, the results from the present study begin to produce a conceptual model for the nature of peripheral vascular disease in the metabolic syndrome. At this age in OZR (∼17 weeks), where we have failed to demonstrate consistent alterations to skeletal muscle function *per se*, impairments to the ability of skeletal muscle to resist fatigue appear to predominantly represent perfusion-based constraints. While there is a component of the poor outcomes that results from bulk ischemia to the contracting muscle, interventions that improve bulk blood flow alone are minimally effective in terms of improving muscle performance (12). Additionally, interventions targeted at improving vascular endothelial function are also of limited effectiveness in terms of improving muscle performance (12). However, imposition of both interventions can restore a significant percentage of the reduction to muscle performance (12), and this is associated both an increase in bulk perfusion to the muscle and an improved perfusion:demand matching in the

distal microcirculation, as well as oxygen extraction and VO_2. Under resting conditions, the increased γ at arteriolar bifurcations in OZR, combined with its increased temporal stability (5), creates an increased number of stable 'low flow/low hematocrit' microvascular pathways in OZR that are not present in LZR. If this condition persists during periods of elevated metabolic demand, it may represent a major contributor to the accelerated muscle fatigue determined in OZR versus LZR. While pharmacological intervention can improve resting H_{MV} and reverse these perfusion-based contributors to poor functional outcome, the loss of microvascular surface area for exchange as a result of the progressive rarefaction that develops in parallel to the hemodynamic impairments could represent an additional source of constraint on skeletal muscle performance.

Limitations

The most significant limitation of the current study is that the measurements have been made under resting conditions. As such, one must be cautious to avoid over-interpreting these results in terms of their relevance for the development of muscle fatigue. At present, we have compelling correlative evidence that demonstrated alterations to microvascular perfusion distribution, microvascular hematocrit and oxygen flux, can be improved with interventions and could contribute to an improved muscle fatigue resistance. In addition, we have recently demonstrated that increasing concentrations of adenosine (as a proxy for elevated metabolic demand) can also blunt the spatial-temporal impairments to microvascular perfusion distribution. However, owing to technical challenges, the effects of imposed muscle contraction and elevated metabolic demand on γ and on microvascular hematocrit has not been directly investigated to date. Addressing this limitation represents a significant challenge that must be overcome in order to facilitate the continued acquisition of novel insight.

Perspectives

Armed with this novel insight into the true nature of peripheral vascular disease in this model, future experiments should target interventional strategies that will either blunt the development of the identified impairments to muscle perfusion/performance or begin the process reversing them once they have begun to develop. At this time, this should take two forms. The first of these is the development of physiologically-realistic, mechanistically accurate models for peripheral vascular disease in OZR, such that better defined, targeted experiments can be developed. The second of these is the incorporation of human subject research, such that the translational relevance and importance of these results can be determined in afflicted human subjects. If this is demonstrated to be translationally accurate, the use of accurate computational models could be exploited for the improved targeting of therapeutic efforts.

Acknowledgments

This study was supported by the American Heart Association (IRG 14330015), the National Institutes of Health (RR 2865AR, P20 GM103434, T32 HL 90610). Additionally, we acknowledge the support provided through Center for Cardiovascular and Respiratory Sciences at the West Virginia University Health Sciences Center. The authors also express their gratitude to Dr. Stephanie J. Frisbee from the West Virginia University School of Public Health for her expert guidance regarding statistical analyses.

References

1. Aleixandre de Artiñano A, Miguel Castro M. Experimental rat models to study the metabolic syndrome. Br J Nutr. 2009 Nov; 102(9):1246–53. [PubMed: 19631025]
2. Bassingthwaighte JB, Goresky CA. Modeling in the analysis of solute and water exchange in the microvasculature. Handbook of Physiology Sect 2, The Cardiovascular System Vol IV, The Microcirculation. 1984:549–626.
3. Bonora E, Targher G, Formentini G, Calcaterra F, Lombardi S, Marini F, Zenari L, Saggiani F, Poli M, Perbellini S, Raffaelli A, Gemma L, Santi L, Bonadonna RC, Muggeo M. The Metabolic Syndrome is an independent predictor of cardiovascular disease in Type 2 diabetic subjects. Prospective data from the Verona Diabetes Complications Study. Diabet Med. 2004 Jan; 21(1):52–8. [PubMed: 14706054]
4. Brigham KL, Faulkner SL, Fisher RD, Bender HW Jr. Lung water and urea indicator dilution studies in cardiac surgery patients. Comparisons ofmeasurements in aortocoronary bypass and mitral valve replacement. Circulation. 1976 Feb; 53(2):369–76. [PubMed: 1106909]
5. Butcher JT, Goodwill AG, Stanley SC, Frisbee JC. Blunted temporal activity of microvascular perfusion heterogeneity in metabolic syndrome: a new attractor for peripheral vascular disease? Am J Physiol Heart Circ Physiol. 2013 Feb 15; 304(4):H547–58. [PubMed: 23262133]
6. Clapauch R, Mecenas AS, Maranhão PA, Bouskela E. Microcirculatory function in postmenopausal women: role of aging, hormonal exposure and metabolic syndrome. Microvasc Res. 2009 Dec; 78(3):405–12. [PubMed: 19695269]
7. Cousineau D, Rose CP, Lamoureux D, Goresky CA. Changes in cardiac transcapillary exchange with metabolic coronary vasodilation in the intact dog. Circ Res. 1983 Dec; 53(6):719–30. [PubMed: 6357532]
8. Desjardins C, Duling BR. Heparinase treatment suggests a role for the endothelial cell glycocalyx in regulation of capillary hematocrit. Am J Physiol. 1990 Mar; 258(3 Pt 2):H647–54. [PubMed: 2316679]
9. Desjardins C, Duling BR. Microvessel hematocrit: measurement and implications for capillary oxygen transport. Am J Physiol. 1987 Mar; 252(3 Pt 2):H494–503. [PubMed: 3548438]
10. Duvnjak L, Duvnjak M. The metabolic syndrome - an ongoing story. J Physiol Pharmacol. 2009 Dec; 60(Suppl 7):19–24. [PubMed: 20388942]
11. Fellmann L, Nascimento AR, Tibiriça E, Bousquet P. Murine models for pharmacological studies of the metabolic syndrome. Pharmacol Ther. 2013 Mar; 137(3):331–40. [PubMed: 23178510]
12. Frisbee JC, Goodwill AG, Butcher JT, Olfert IM. Divergence between arterial perfusion and fatigue resistance in skeletal muscle in the metabolic syndrome. Exp Physiol. 2011 Mar; 96(3): 369–83. [PubMed: 21123363]
13. Frisbee JC, Wu F, Goodwill AG, Butcher JT, Beard DA. Spatial heterogeneity in skeletal muscle microvascular blood flow distribution is increased in the metabolic syndrome. Am J Physiol Regul Integr Comp Physiol. 2011 Oct; 301(4):R975–86. [PubMed: 21775645]
14. Frisbee JC. Remodeling of the skeletal muscle microcirculation increases resistance to perfusion in obese Zucker rats. Am J Physiol Heart Circ Physiol. 2003 Jul; 285(1):H104–11. [PubMed: 12649071]
15. Fry BC, Roy TK, Secomb TW. Capillary recruitment in a theoretical model for blood flow regulation in heterogeneous microvessel networks. Physiol Rep. 2013 Aug.1(3):e00050. [PubMed: 24040516]
16. Gauden V, Hu DE, Kurokawa T, Sarker MH, Fraser PA. Novel technique for estimating cerebrovascular permeability demonstrates capsazepine protection following ischemia-reperfusion. Microcirculation. 2007 Nov-Dec;14(8):767–78. [PubMed: 17907014]
17. House SD, Lipowsky HH. Microvascular hematocrit and red cell flux in rat cremaster muscle. Am J Physiol. 1987 Jan; 252(1 Pt 2):H211–22. [PubMed: 3812711]
18. Keller KB, Lemberg L. Obesity and the metabolic syndrome. Am J Crit Care. 2003 Mar; 12(2): 167–70. [PubMed: 12625176]
19. Keller MW, Damon DN, Duling BR. Determination of capillary tube hematocrit during arteriolar microperfusion. Am J Physiol. 1994 Jun; 266(6 Pt 2):H2229–38. [PubMed: 7517645]

20. Kocsis L, Herman P, Eke A. Mathematical model for the estimation of hemodynamic and oxygenation variables by tissue spectroscopy. J Theor Biol. 2006 Jul 21; 241(2):262–75. [PubMed: 16413035]
21. Lombard JH, Hinojosa-Laborde C, Cowley AW Jr. Hemodynamics and microcirculatory alterations in reduced renal mass hypertension. Hypertension. 1989 Feb; 13(2):128–38. [PubMed: 2914735]
22. Overholser KA, Lomangino NA, Harris TR, Bradley JD, Bosan S. Deduction of pulmonary microvascular hematocrit from indicator dilution curves. Bull Math Biol. 1994 Mar; 56(2):225–47. Erratum in: Bull Math Biol 1995 Nov;57(6):931. [PubMed: 8186753]
23. Padilla DJ, McDonough P, Behnke BJ, Kano Y, Hageman KS, Musch TI, Poole DC. Effects of Type II diabetes on capillary hemodynamics in skeletal muscle. Am J Physiol Heart Circ Physiol. 2006; 291:H2439–44. [PubMed: 16844923]
24. Padilla DJ, McDonough P, Behnke BJ, Kano Y, Hageman KS, Musch TI, Poole DC. Effects of Type II diabetes on muscle microvascular oxygen pressures. Respir Physiol Neurobiol. 2007; 156(2):187–95. [PubMed: 17015044]
25. Poole DC, Hirai DM, Copp SW, Musch TI. Muscle oxygen transport and utilization in heart failure: implications for exercise (in)tolerance. Am J Physiol Heart Circ Physiol. 2012; 302:H1050–63. [PubMed: 22101528]
26. Potenza MV, Mechanick JI. The metabolic syndrome: definition, global impact, and pathophysiology. Nutr Clin Pract. 2009 Oct-Nov;24(5):560–77. [PubMed: 19841245]
27. Pries AR, Ley K, Gaehtgens P. Generalization of the Fahraeus principle for microvessel networks. Am J Physiol. 1986 Dec; 251(6 Pt 2):H1324–32. [PubMed: 3789184]
28. Pries AR, Secomb TW, Gaehtgens P, Gross JF. Blood flow in microvascular networks. Experiments and simulation. Circ Res. 1990 Oct; 67(4):826–34. [PubMed: 2208609]
29. Richardson TE, Kindig CA, Musch TI, Poole DC. Effects of chronic heart failure on skeletal muscle capillary hemodynamics at rest and during contractions. J Appl Physiol. 2003; 95:1055–62. [PubMed: 12740313]
30. Smolock CJ, Anaya-Ayala JE, Bismuth J, Naoum JJ, El Sayed HF, Peden EK, Lumsden AB, Davies MG. Impact of metabolic syndrome on the outcomes of superficial femoral artery interventions. J Vasc Surg. 2012 Apr; 55(4):985–993. [PubMed: 22341577]
31. Stainsby WN, Snyder B, Welch HG. A pictographic essay on blood and tissue oxygen transport. Med Sci Sports Exerc. 1988 Jun; 20(3):213–21. [PubMed: 3386498]

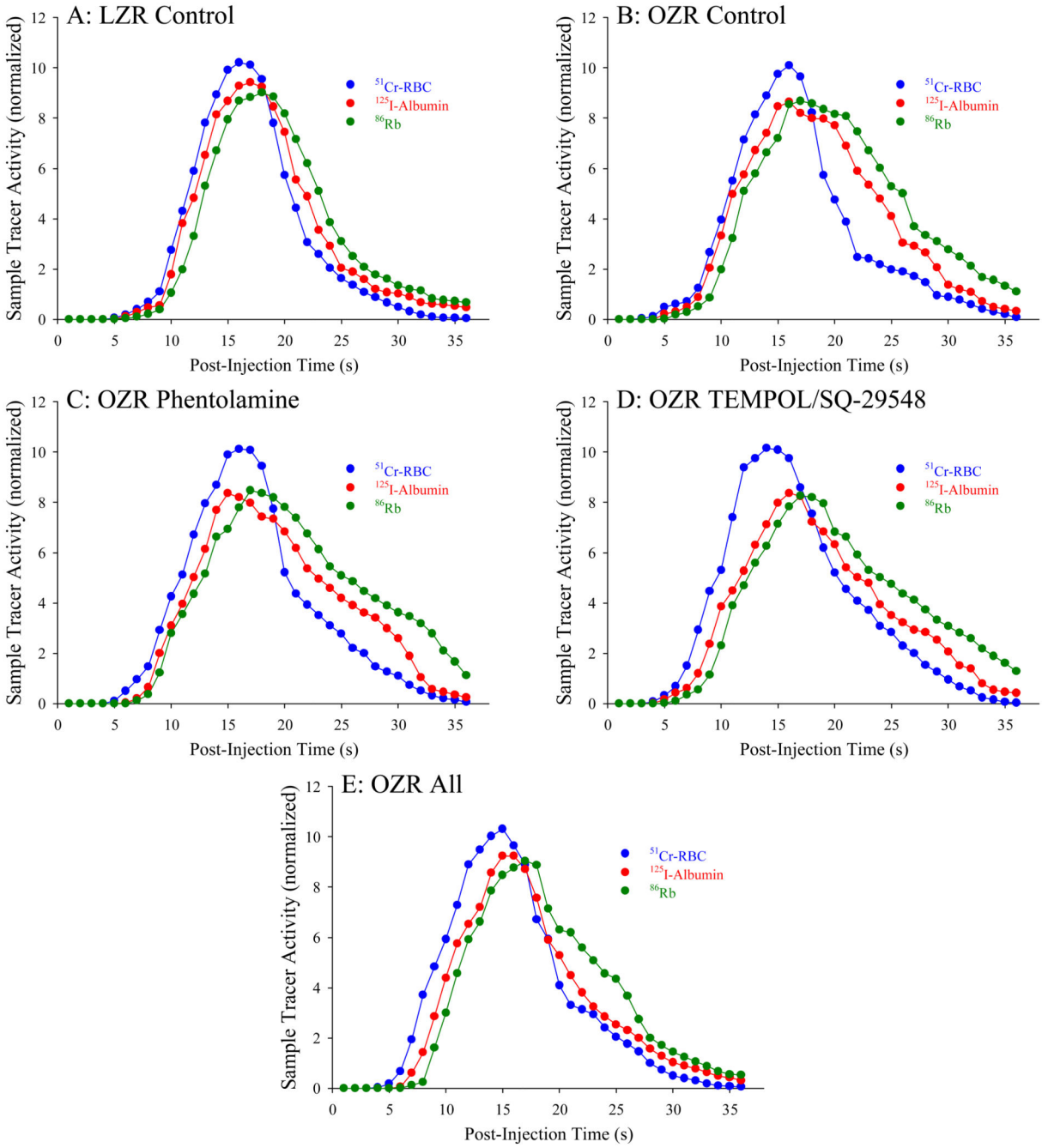

Figure 1.

Representative tracer washout curves following bolus intra-arterial injection proximal to the *in situ* gastrocnemius muscle from LZR and OZR under the conditions of the present study. Data are presented for LZR – Control (Panel A), and OZR – Control (Panel B) and following pre-treatment of OZR with phentolamine (Panel C), TEMPOL and SQ-29548 (Panel D) and all three agents (Panel E). Please see text for details.

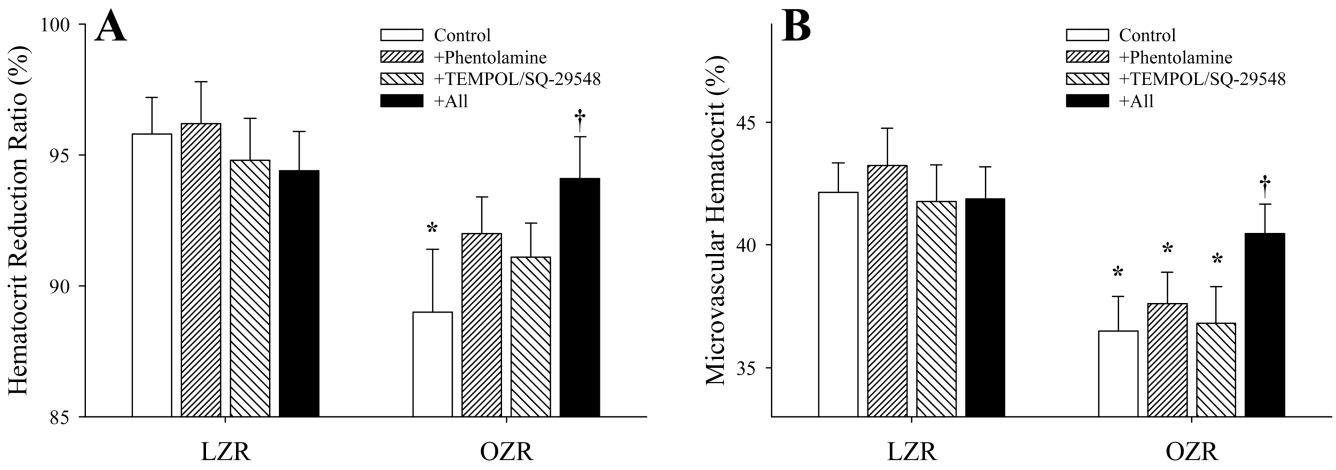

Figure 2.

Calculated hematocrit reduction ratio (%; Panel A) and aggregate microvascular hematocrit (%, Panel B) in the *in situ* gastrocnemius muscle of LZR and OZR under the conditions of the current study. Calculations are based on the analyses of the tracer washout curves, representative washout curves are presented in Figure 1. Data are presented as mean±SE, * $p<0.05$ versus LZR-Control, † $p<0.05$ versus OZR-Control. For LZR, n=6 for Control, n=3 for Phentolamine, n=3 for TEMPOL/SQ-29548 and n=6 for all. For OZR, n=17 for Control, n=8 for Phentolamine, n=9 for TEMPOL/SQ-29548 and n=17 for all. Please see text for details.

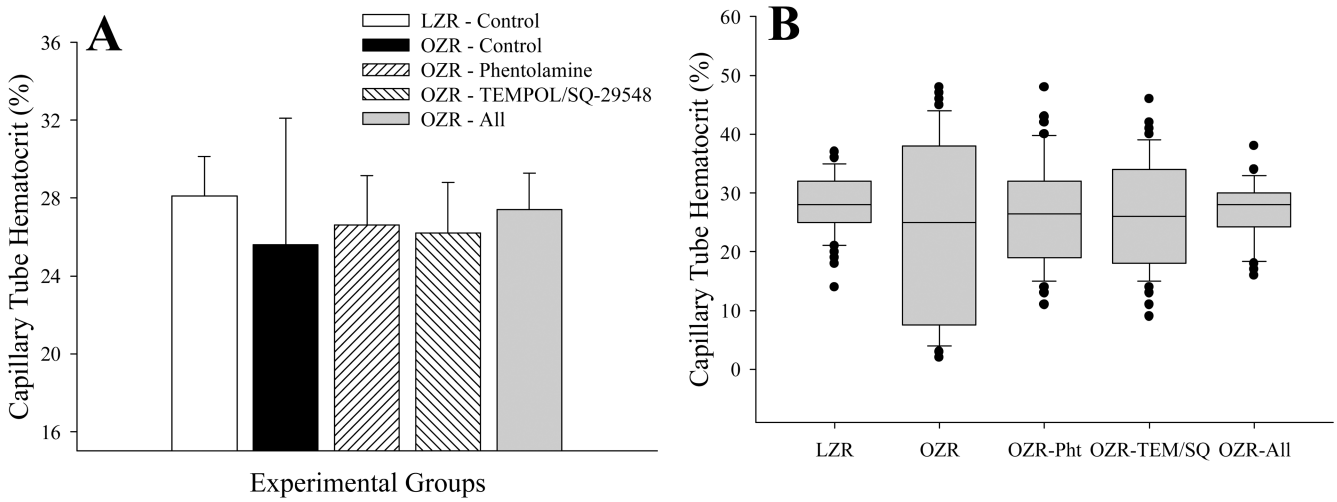

Figure 3.

Capillary tube hematocrit in microvessels from LZR and OZR under the conditions of the present study. Calculations are made from individual microvessels from a trans-illuminated *in situ* cremaster muscle from LZR and OZR. Data are presented as mean±SE. Panel A presents aggregate for H_T, while Panel B presents the data as a 'box-and-whisker' plot, where The bottom boundary of the box indicates the 25th percentile, a central line within the box marks the median, and the upper boundary of the box indicates the 75th percentile. Whiskers are represented as the error bars above and below the box and represent the 90th and 10th percentiles. H_T values in Panel A are based on 10 measurements/animal, with n=6 for LZR and 8-10 for OZR. Please see text for details.

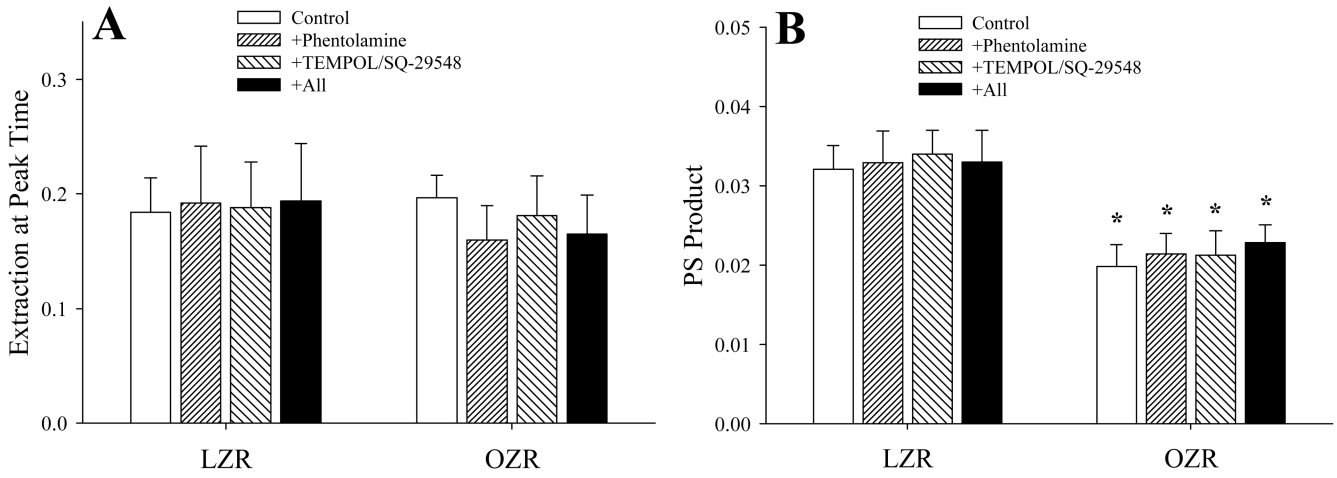

Figure 4.

Data describing the calculated extraction (Panel A) and permeability-surface area product (PS; Panel B) across the *in situ* gastrocnemius muscle of LZR and OZR under the conditions of the current study. Calculations are based on the analyses of the tracer washout curves, representative washout curves are presented in Figure 1. Data are presented as mean±SE, * $p<0.05$ versus LZR-Control. For LZR, n=6 for Control, n=3 for Phentolamine, n=3 for TEMPOL/SQ-29548 and n=6 for all. For OZR, n=17 for Control, n=8 for Phentolamine, n=9 for TEMPOL/SQ-29548 and n=17 for all. Please see text for details.

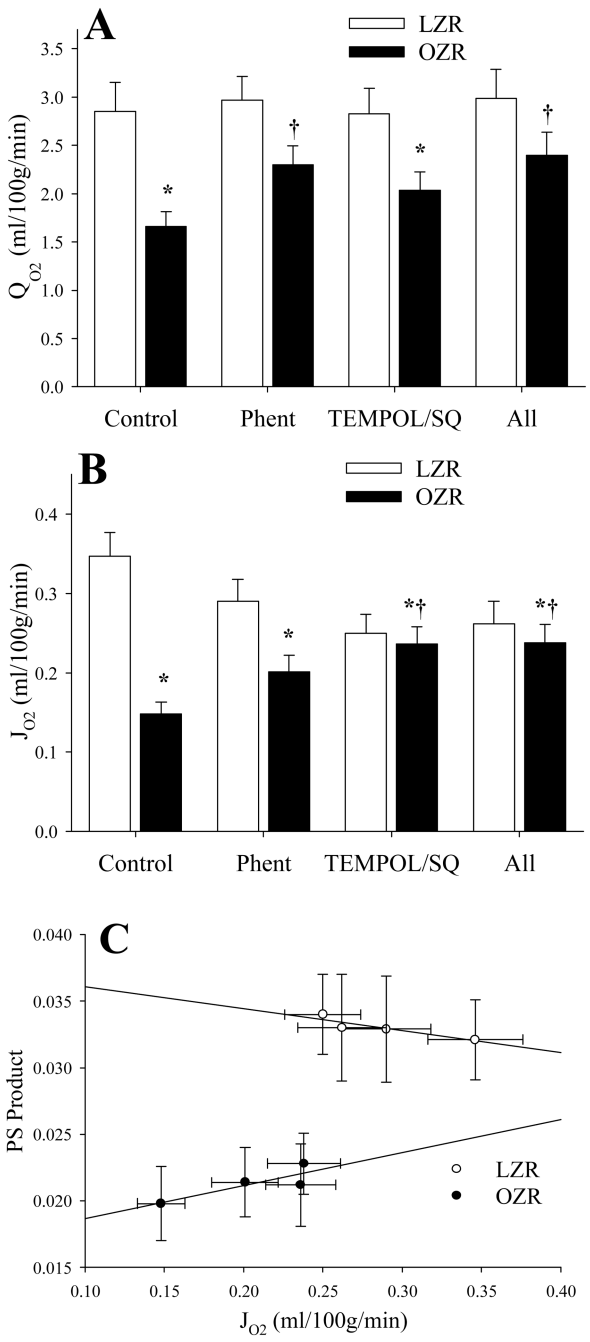

Figure 5.

Data describing perfusive oxygen flux (Q_{O2}; Panel A), diffusive oxygen flux (J_{O2}; Panel B) and the correlation between J_{O2} and PS Product (Panel C) under the conditions of the present study. In Panel C, the equation for the relationship in LZR is:$y = 0.0377 + 0.0165\chi$; $r^2=0.819$, while for OZR this relationship is: $y = 0.0162 + 0.0248\chi$; $r^2=0.721$. * $p<0.05$ vs. LZR Control, † $p<0.05$ vs. OZR Control.

Table 1

Baseline characteristics between LZR and OZR in the present study. All rats are male, aged ∼17 weeks.

	LZR	OZR
Mass (g)	358±10	694±16*
MAP (mmHg)	103±5	128±6*
$Insulin_{plasma}$ (ng/ml)	1.4±0.2	8.4±0.8*
$Glucose_{blood}$ (mg/dl)	88±9	168±12*
$Nitrotyrosine_{plasma}$ (ng/ml)	14±4	47±8*

* $p<0.05$ versus LZR.

Table 2

Blood oxygen tensions and contents and bulk blood flow (ml/100g/min) for *in situ* skeletal muscle of LZR and OZR under the conditions of the present study. Blood flow was normalized based on the perfused gastrocnemius muscle mass, which was not significantly different between the two strains (LZR=2.21±0.07 g; OZR=2.14±0.08 g).

Condition	Variable	LZR	OZR
Control	Flow (ml/100g/min)	12.9±1.1	7.8±0.8*
	PaO_2 (mmHg)	97±1	96±1
	PvO_2 (mmHg)	58±3	64±3
	CaO_2 (ml/ml blood)	0.220±0.01	0.219±0.01
	CvO_2 (ml/ml blood)	0.193±0.02	0.199±0.02
Phentolamine	Flow (ml/100g/min)	13.4±0.9	10.4±1.0†
	PaO_2 (mmHg)	97±1	97±1
	PvO_2 (mmHg)	65±2	66±3
	CaO_2 (ml/ml blood)	0.221±0.01	0.221±0.01
	CvO_2 (ml/ml blood)	0.199±0.02	0.201±0.02
TEMPOL/SQ	Flow (ml/100g/min)	12.8±1.0	9.1±0.7
	PaO_2 (mmHg)	95±1	96±1
	PvO_2 (mmHg)	64±2	58±2
	CaO_2 (ml/ml blood)	0.218±0.01	0.219±0.01
	CvO_2 (ml/ml blood)	0.199±.0.02	0.193±0.02
All	Flow (ml/100g/min)	13.5±1.1	10.8±0.9†
	PaO_2 (mmHg)	97±1	97±1
	PvO_2 (mmHg)	66±2	64±2
	CaO_2 (ml/ml blood)	0.221±0.01	0.221±0.01
	CvO_2 (ml/ml blood)	0.201±.0.02	0.199±0.02

*p<0.05 versus LZR Control;

†p<0.05 vs. OZR Control.